

# Lipid Bilayer Templated Gold Nanoparticles Nanoring Formation Using Zirconium Ion Coordination Chemistry

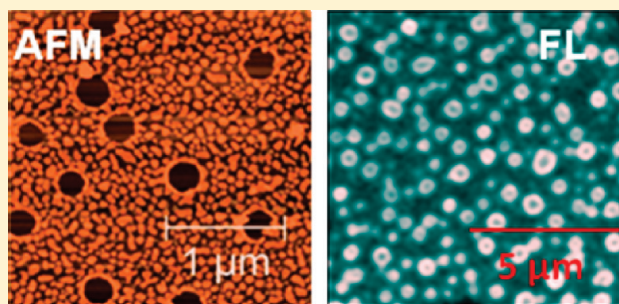
Xiaoyin Xiao,<sup>†</sup> Gabriel A. Montaña,<sup>‡</sup> Amy Allen,<sup>†</sup> Komandoor E. Achyuthan,<sup>†</sup> David R. Wheeler,<sup>†</sup> and Susan M. Brozik<sup>\*,†</sup>

<sup>†</sup>Biosensors and Nanomaterials Department, Sandia National Laboratories, Albuquerque, New Mexico 87185, United States

<sup>‡</sup>Center for Integrated Nanotechnologies, Los Alamos National Laboratory, Los Alamos, New Mexico 87545, United States

**S** Supporting Information

**ABSTRACT:** We used positively charged lipids to prepare lipid bilayer assemblies (LBAs) upon which we assembled negatively charged gold nanoparticles (AuNPs). Treatment of the assembly with zirconium chloride resulted in the formation of nanorings of the diameters inversely related to the zirconium ion concentration. The nanorings were attributed to the zirconium ion coordinated AuNPs formed during the lipid bilayer budding process promoted by the acid effect of zirconium chloride. Nanoring organization was also dependent on the fluidity of lipid bilayers, an indication of LBA-assisted nanomaterials organization. We suggest that such bioorganic–inorganic hybrid assemblies coupled to unique topological and morphological variations might be useful as stimuli-responsive sensors or storage compartments for proteins or drugs.



## INTRODUCTION

Lipid bilayer assemblies (LBAs) on solid substrates are widely used to mimic the dynamics and structural features of cell membranes.<sup>1,2</sup> Using LBAs, it is possible to mimic and investigate biologically relevant processes such as membrane protein recognition and channel function as well as use the LBAs for biomaterials or biomedical applications. For example, biosensors can be created by the incorporation of ion channel proteins as well as other membrane protein receptors.<sup>3–6</sup> The formation of LBAs on solid supports typically occurs with a 10–20 Å thick hydration layer between the bilayer and the support (substratum) affording the LBAs lateral fluidity.<sup>7,8</sup> Accordingly, while supported, the LBAs are typically able to maintain their intrinsic structural and functional properties. This is illustrated by examples of lipids such as palmitoyl oleoyl phosphatidylcholine (POPC) and *N*-[1-(2,3-dioleoyloxy)propyl]-*N,N,N*-trimethylammonium methylsulfate (DOTAP) with solid phase transition temperatures below room temperature that result in fluid LBAs at room temperature, whereas saturated lipids such as distearylphosphatidylcholine (DSPC) result in nonfluid LBAs at room temperature. Likewise, a combination of two or more lipid mixtures can result in two-dimensional phase separation of the various lipid components.<sup>9,10</sup> Although the supported bilayers can be assembled upon a variety of solid surfaces by vesicle fusion and Langmuir–Blodgett techniques, their detailed structures are often complex and strongly related to the lipid composition, the nature of the surface, and assembly conditions such as temperature, ionic strength, and pH.<sup>11</sup>

Depending on the environmental conditions used, phenomena such as bilayer curvature and formation of nanodomains and nanopores have been observed.<sup>12–17</sup> Other work has focused upon the interactions of synthetic organic and inorganic nanoparticles (NPs) with biological membranes.<sup>18–21</sup> Synthetic NPs such as particles of noble metals (e.g., Pt, Au, and Ag), chemically modified fullerenes, poly(amidoamine) dendrimers, and quantum dots have been investigated for potential applications such as drug delivery, gene therapy, and nanomedicines. However, research has also suggested that NPs can have potential adverse effects to human health due to mechanisms such as membrane disruption and lipid peroxidation.<sup>22,23</sup> Other studies have reported conflicting results regarding the extent and effects of NP interactions with cellular membranes.<sup>24</sup> Regardless, it is becoming apparent that there is potential for designing and tuning the interactions of NPs with LBAs as well as cell-derived lipid membranes. Here we report the organization of carboxylic acid terminated gold nanoparticles (AuNPs) that interact with a positively charged DOTAP lipid bilayer membrane. The AuNPs are shown to organize into nanoring architectures due to a combination of zirconium coordination chemistry<sup>25</sup> and secondary acidic disruption of the LBA due to addition of ZrCl<sub>4</sub>. Potential applications of these nanoring structures are briefly discussed.

**Received:** April 21, 2011

**Revised:** May 26, 2011

**Published:** June 23, 2011

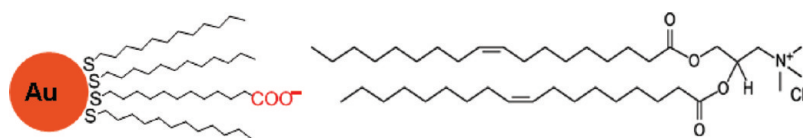


**Figure 1.** Schematics of negatively charged AuNP and positively charged DOTAP lipid.

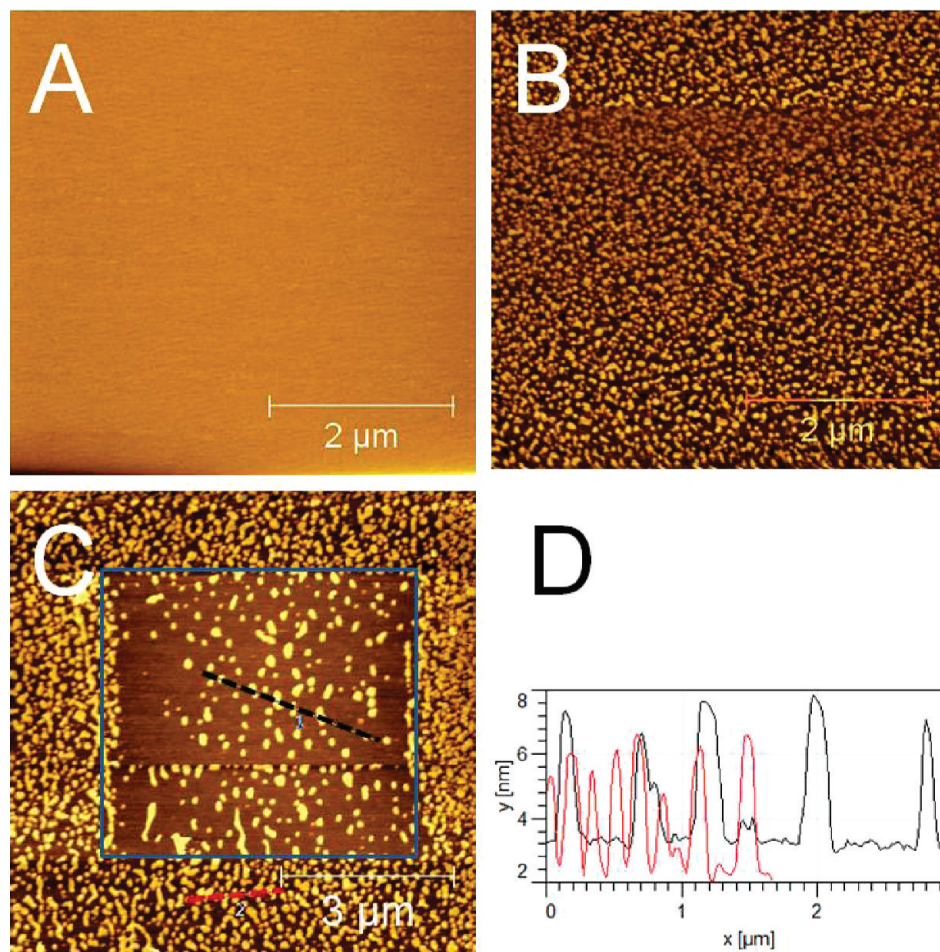


**Figure 2.** AFM images of DOTAP bilayer before (A) and after (B) the addition of pc-AuNPs ( $\sim 1$  nM). (C) AFM image showing pc-AuNPs being pushed away from the center square by an AFM tip and (D) the height analysis along the lines shown in (C).

## EXPERIMENTAL SECTION

**AuNPs Synthesis.** AuNPs were prepared using published methods with minor modifications.<sup>26,27</sup> 1-Dodecanethiol coated AuNPs (i.e., AuNP-DDT) were prepared using a two-phase liquid–liquid reaction system.<sup>26</sup> The fully carboxylated AuNPs (fc-AuNPs), such as 11-mercaptoundecanoic anion and 3-mercaptopropionic acid coated AuNPs (i.e., Au-MUA and Au-MPA, respectively), were prepared by inverse microemulsion method.<sup>27</sup> The partially carboxylated AuNPs (pc-AuNPs) were obtained after ligand exchange reaction between DTT and MUA. The detailed preparation procedures and data of transmission electron microscopy (TEM), dynamic light scattering (DLS), and UV–vis are provided in the Supporting Information.

**Lipids and Liposomes.** Lipids, DOTAP, DSPC, and POPC were purchased from Avanti Polar Lipids and stored in chloroform. Liposomes were prepared by probe sonication. A total of 20 mg of lipid powder was dissolved in 1 mL of chloroform. Further, 76  $\mu$ L of such solution was dried under nitrogen stream and under house-vacuum for

more than 2 h. The lipid cake was then hydrated with *N*-(2-hydroxyethyl)piperazine-*N'*-(2-ethanesulfonic acid) (HEPES) buffer (150 mM NaCl + 20 mM CaCl<sub>2</sub> + 10 mM HEPES, pH 7.4). After five freeze–thaw cycles, the solution was probe sonicated for 10 min. The size of liposomes was fairly monodisperse around 30–40 nm.

**Lipid Bilayer Assembly.** Supported lipid bilayers were assembled by placing liposome solutions on freshly cleaved mica or piranha (3:1 concentrated sulfuric acid to 30% hydrogen peroxide solution) cleaned glass coverslips. The bilayers were first rinsed with water and then Tris-HCl buffer (50 mM Tris, pH 8.2).

**AuNPs Binding.** Fully and partially carboxylated AuNPs were dissolved in Tris buffer, pH 8.2, and were directly introduced onto the supported lipid bilayers by electrostatic interaction. Above 1 nM of particle concentration, the particle coverage reached saturation.

**HCl or ZrCl<sub>4</sub> Treatment.** After binding AuNPs, usually for 10–30 min after introducing particle solutions, the surfaces were then rinsed with Tris buffer and water to remove unbound particles. The solution was then exchanged by 0.01–0.1 M HCl or 0.005–0.1 M ZrCl<sub>4</sub> twice. In

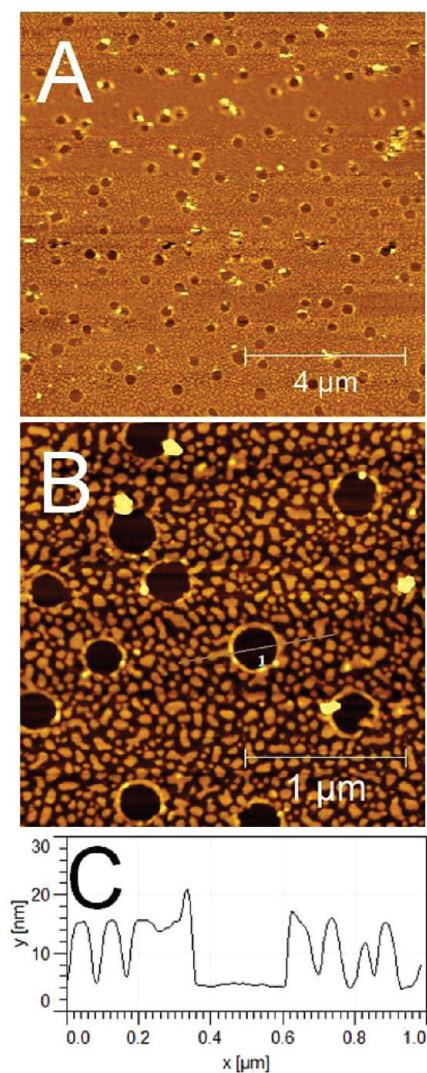


**Figure 3.** (A,B) AFM images of the nanorings formed after addition of 5 mM  $\text{ZrCl}_4$  to the DOTAP bilayer covered with pc-AuNPs. (C) Height analysis along the line shown in (B).

AFM experiments, the acidic solutions were then exchanged to DI-water followed by Tris buffer for imaging. In fluorescence experiments, the samples were directly imaged in the presence of HCl or  $\text{ZrCl}_4$ .

**Atomic Force Microscopy (AFM).** We used Agilent Pico SPM II and MAC Type II cantilevers with a typical spring constant of  $\sim 1$  N/m. All images were taken in a liquid cell in MAC mode (set point,  $\sim 75\%$  of free oscillation; scan rate,  $\sim 1$  Hz). To mechanically scratch the particle/lipid bilayer surfaces, the set point was further decreased to  $\sim 30\%$  of free oscillation. Image analysis was performed using Gwyddion software.

**Fluorescence Microscopy.** We used an Olympus IX-71 inverted optical microscope to generate a TIF file of the fluorescence image and then analyzed the image using Gwyddion software for the scale bar, color and color scale, and optical dimensions of the nanorings. A concentration of 0.3% of  $\beta$ -BODIPY FL  $\text{C}_{12}$ -HPC (Invitrogen, Life Technologies, Carlsbad, CA) in lipid bilayers was used. The dye had excitation and emission maxima of 506 and 513 nm, respectively.

## RESULTS AND DISCUSSION

**AuNPs Assembly.** The core diameter of both fc-AuNPs and pc-AuNPs was 3–5 nm, and their hydrodynamic size around 10 nm as determined by TEM and DLS, respectively.

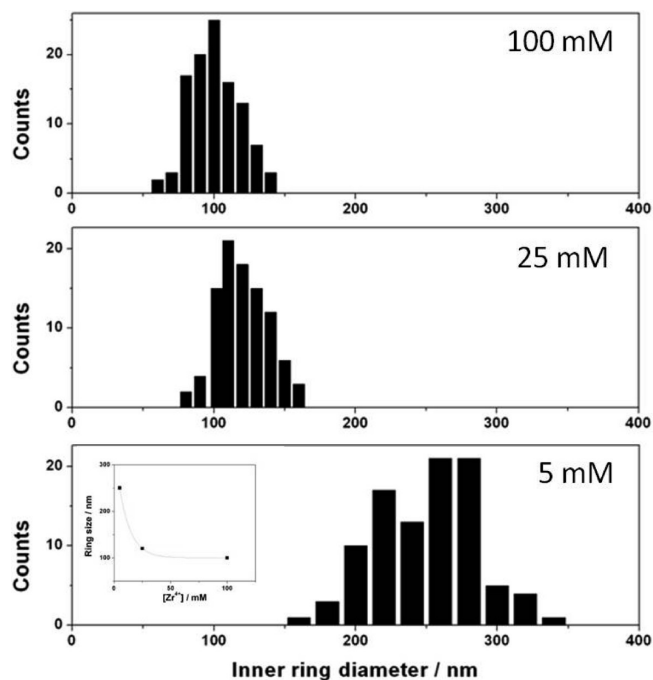


**Figure 4.** Dependence of nanoring size distribution on zirconium ion concentration.

The absorption peak of the pc-AuNPs was at  $\sim 512$  nm. AuNPs coated by a pure monolayer of MUA or MPA had an absorption maximum of  $\sim 532$  nm (Figure S1 of the Supporting Information). The particles were soluble at pH greater than 7.0 and were stable for several months.

Initially, we attempted to assemble the AuNPs onto DOTAP LBAs using fully carboxylated AuNPs, Au-MUA, or Au-MPA, based on the electrostatic attraction between the oppositely charged lipid headgroup and the AuNPs. However, we found that these negatively charged AuNPs often disrupted or peeled off the positively charged DOTAP membranes, similar to the observations made by others.<sup>28,29</sup> We therefore synthesized partially carboxylated AuNPs with much less surface charge and assembled these particles on the LBA. Figure 1 illustrates the proposed molar ratio between MUA and DDT molecules adsorbed at the AuNP surfaces. DOTAP is a cationic lipid with a net positively charged headgroup. Figure 2A shows a typical AFM image of a DOTAP bilayer on mica before pc-AuNPs were assembled. The image is almost featureless, since the DOTAP bilayer remains fluidic at room temperature. Figure 2B shows the DOTAP LBA after addition of 1 nM pc-AuNP solution at pH  $\sim 8$ . The spherical nanoparticles of rather uniform size distribution are observed on the LBA surface with no disruption of the underlying LBA. We found that pc-AuNPs did not assemble on the POPC bilayers presumably due to a net zero surface charge. The surface coverage of AuNPs was also shown to be controllable by varying particle concentrations or replacing the DOTAP partially by POPC and DSPC which are zwitterionic lipids with zero net surface charges.

The electrostatic interactions between DOTAP bilayers and pc-AuNPs were investigated by AFM. Figure 2B is a typical surface of pc-AuNPs assembled on the DOTAP bilayer. After an initial scan of such a surface area under a rather large force, that is, scanning the surface at an amplitude set point  $\sim 30\%$  of the free oscillating amplitude, a second, larger area scan at normal 75% of

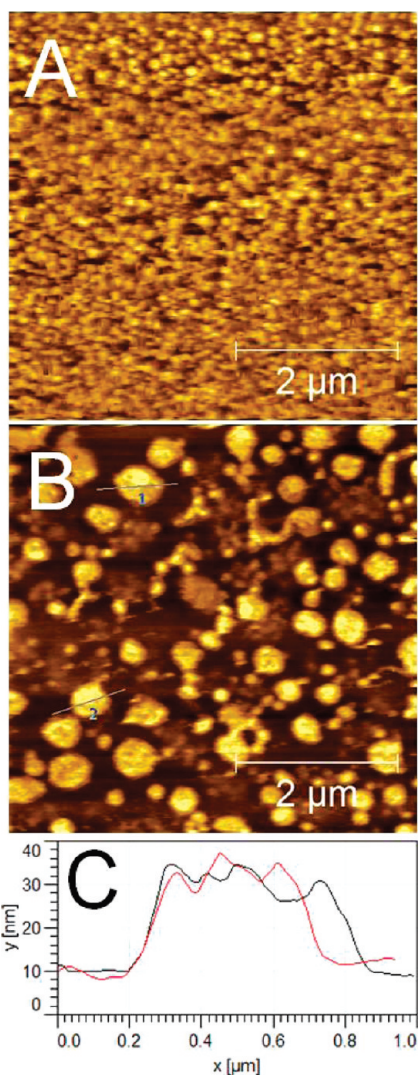


**Figure 5.** AFM images of the DOTAP bilayer covered with pc-AuNPs before (A) and after (B) the addition of 10 mM HCl. (C) Height analysis along the lines shown in (B).

the free oscillating amplitude was taken (Figure 2C). As can be observed, most of the pc-AuNPs have been pushed away by the AFM tip during the initial scan, leaving a sparsely covered DOTAP LBA in the area of the previous scan. The LBA appears to remain intact upon both pc-AuNP deposition and forced movement within the detection limit of AFM. Figure 2D shows that the particles are about 5 nm above the bilayer, which is close to the hydrodynamic radius of pc-AuNPs measured by DLS.

**Zr Ion Induced Nanoring Formation.**  $\text{ZrCl}_4$  has the potential to coordinate with the carboxylic groups on the functionalized AuNPs. Figure 3A shows that  $\sim 250$  nm inner diameter sized nanorings were formed immediately after 5 mM  $\text{ZrCl}_4$  solution was added. Figure 3B and the corresponding phase image (Figure S2 of the Supporting Information) indicate that the underlying bilayer appeared to be unaltered. The inside of the nanorings is as flat as previous fluidic bilayer surfaces. The AFM height analysis still shows 6–10 nm in height difference corresponding to the radius of AuNPs (Figure 3C). In addition to nanoring formation, the rest of the bilayer was covered by individual

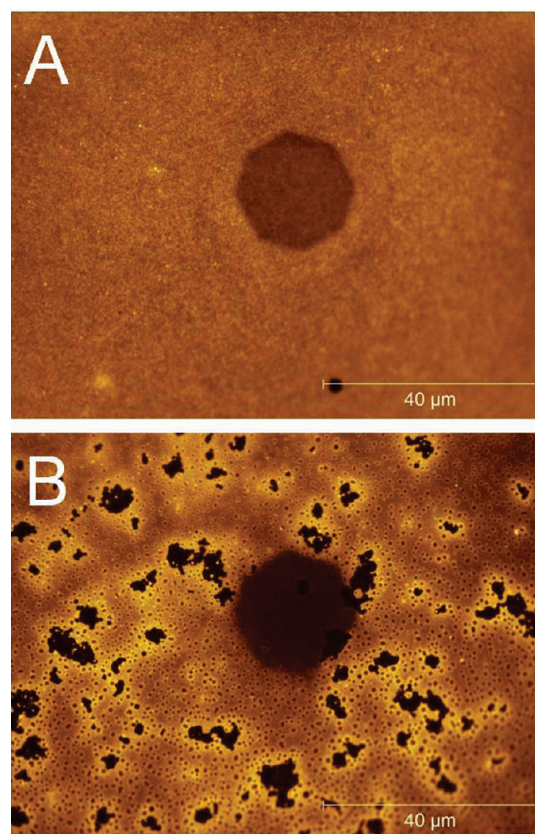


**Figure 6.** Fluorescence images of a DOTAP bilayer on glass before (A) and after (B) the addition of 5 mM  $\text{ZrCl}_4$  in the absence of AuNPs.

particles or relatively larger islands, an indication of short-distance limited reorganization of AuNPs.

We have examined and found several experimental conditions that affected the formation of nanorings. First, the diameter of the nanorings was decreased when a higher concentration of  $\text{ZrCl}_4$  was used. Figure 4 shows the size distribution of the nanorings analyzed from three to four surface locations for three Zr ion concentrations. The ring sizes were inversely related to Zr ion concentration. Second, the addition of  $\text{ZrCl}_4$  in the presence of acetic acid, that is, Zr ions were fully coordinated with acetate, did not lead to any ring formation (Figure S3 of the Supporting Information), suggesting that free Zr ions were needed to coordinate with carboxylic groups among the AuNPs. Third, the addition of Cu or Ni ions, instead of Zr ions, did not result in nanoring formation. Fourth, nanorings were not formed when DOTAP was partially replaced by DSPC at more than 20%, indicating that bilayer fluidity plays a role in ring formation. Finally, when the Zr ion solutions were carefully buffered at pH above 3, no nanorings were observed. The dependence of ring formation on pH indicates that the coordination of Zr ions with carboxylic groups alone is not able to induce AuNP reorganization at pH above 3. The reorganization of AuNPs requires the particles to move above the bilayers, which is possibly hindered by the weakly electrostatic attraction from the lipid head groups.

**Acid-Induced Bilayer Disruption and Budding.** The pH values of the  $\text{ZrCl}_4$  solutions for the three concentrations were 2.06 (5 mM), 1.68 (25 mM), and 1.36 (100 mM). To determine the pH effect in the process of AuNP reorganization, we treated the LBA-pc-AuNPs surface with 0.01 M HCl, pH  $\sim 2.0$ , in the

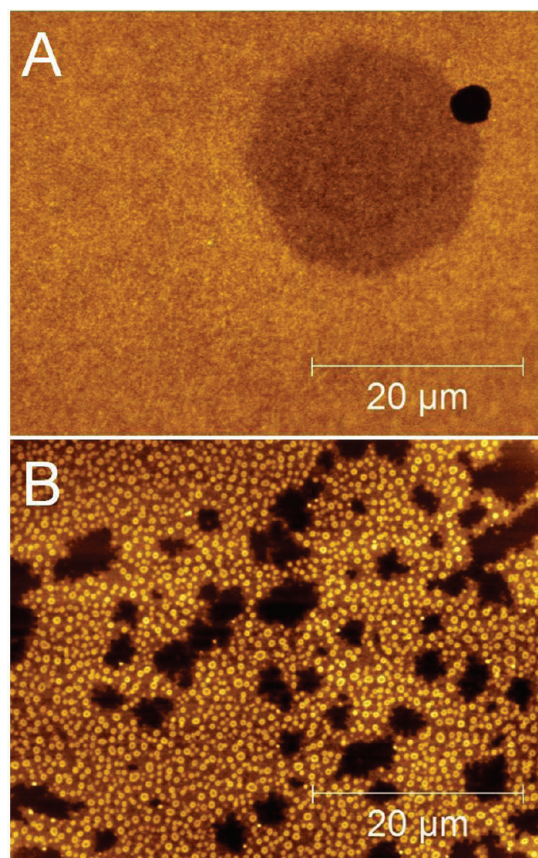


**Figure 7.** Fluorescence images of DOTAP bilayer covered with pc-AuNPs before (A) and after (B) the addition of 5 mM  $ZrCl_4$ .

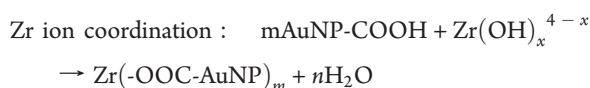
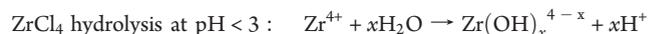
place of unbuffered  $ZrCl_4$  solution. As can be seen from Figure 5B, HCl addition resulted in extensive membrane disruption. The residual disklike patches were possibly covered by AuNP aggregates, leading to the height variations greater than the sum of the bilayer thickness ( $\sim 6$  nm) and the AuNP radius (Figure 5C). In contrast to the case of  $ZrCl_4$  treated LBAs, no ordered ring-structures were formed.

We also investigated the effect of the addition of  $ZrCl_4$  on LBAs alone. Figure 6 shows a typical fluorescence microscopy image of a DOTAP bilayer on glass before and after the addition of 5 mM  $ZrCl_4$ . The addition of  $ZrCl_4$  (pH 2.06) disrupted the DOTAP LBA in two ways, creating large patches in the LBA as well as resulting in the appearance of circular holelike structures of rather uniform sizes (Figure 6B). These holelike structures were confirmed to be three-dimensional (3D) bubbles by adjusting the Z plane of the microscope focus. These 3D bilayer structures are similar to earlier structures created by Hovis and co-workers, and recently by Goertz et al.<sup>30–32</sup> The later work showed very similar 3D structures in POPC bilayers at the extreme low and high pHs. In our case, the formation of 3D bubbles is likely due to the protonation of the glass substratum, which altered the stability of bilayers interacting with the substrates.

To determine the effect of AuNPs on membrane disruption, we further used fluorescence microscopy to look at DOTAP LBAs covered with pc-AuNPs and followed by the same  $ZrCl_4$  treatment. Figure 7 shows the bright nanorings above the lipid bilayers and large area bilayer disruptions as well. Optical examination demonstrated that the ring diameters were  $\sim 300$  nm, which although at

the optical detection limit were nevertheless in agreement with our AFM data (Figure 3), suggesting that they are indeed nanorings of pc-AuNPs. Based upon these data, we concluded that, unlike the bubbles observed in Figures 6B for bilayers treated with  $ZrCl_4$  in the absence of pc-AuNPs, the bright nanorings of pc-AuNPs on DOTAP represented zirconium-coordinated gold nanostructures. The brightness of nanorings in Figure 7 is presumed to be due to local surface plasmon resonance between the pc-AuNPs and the  $\beta$ -BODIPY dye molecules,<sup>33,34</sup> since the absorption maximum of the pc-AuNPs (512 nm) overlapped with the excitation maximum (506 nm) of the dye molecules. The nanorings have higher density or closer package of AuNPs and thus more enhanced fluorescent emissions.

**Proposed Ring Formation Mechanism.** The formation of zirconate ( $ZrO_2$ ) rings was excluded in our acidic test solutions. When dissolved in water,  $ZrCl_4$  is readily hydrolyzed to form a variety of derivatives of the zirconyl, dizirconyl, and similar cationic radicals depending on the acidic environment.<sup>35,36</sup> In general,  $Zr(OH)_4$  or  $ZrO_2$  is formed only at pH above 4, at which pH values we did not observe the formation of nanorings. At lower pH values, the cationic zirconyl monomers (pH < 1) and polymers (pH  $\leq$  4) still strongly coordinate with carboxylic acid by breaking the zirconyl–oxygen–zirconyl bridges in their polymeric complexes.<sup>37,38</sup> In our study (pH < 3), each zirconyl polymeric radical was likely capable of coordinating more than two carboxylic acid termini from the same or neighboring AuNPs, leading to the reorganization of AuNPs in the course of an acid-induced membrane budding event.



Zirconium coordination is required in the process of nanoring formation. Such coordination may lead to enhance the stability of AuNPs above bilayers by holding them together and the stability of the bilayers against acid-induced disruption as well. When the pH decreases in the presence of zirconium coordinated AuNPs, the vesicle budding could only occur in the spaces between the coordinated AuNPs. The net result was the observed nanorings. This mechanism also explains the inverse correlation between the nanoring diameter and the  $ZrCl_4$  concentration. Increased  $ZrCl_4$  concentrations resulted in enhanced AuNP coordination leading to greater stability. Thus, only small vesicles were allowed to form and bud off from the LBA surface. It is not fully understood why both AFM and fluorescence images showed the intact bilayers inside the nanorings. However, it is possible that the bilayer budding was initiated by the acid but eventually did not take place or was suppressed by the nanorings. It is also possible that the nanopores within the DOTAP lipid bilayer are backfilled through the bilayer lateral diffusion or from the bulk solution. Addition of Cu or Ni ions did not result in nanoring formation, since their complexes with carboxylic groups were not stable in low pH solutions.

## CONCLUSIONS

We have demonstrated that a combination of the unique properties of DOTAP LBAs and zirconium coordination chemistry of partially carboxylated AuNPs resulted in the formation

of gold nanoring nanostructures. These structures rely on the native lateral fluidity of the LBAs, the pH response of the LBAs to the  $ZrCl_4$ , and the zirconium coordination of the AuNPs. Our approach to gold nanoring formation utilized coordination chemistry and is therefore a much simpler technique compared to colloidal or nanoimprint lithography for gold nanoring fabrication.<sup>39</sup> Our data also suggest potential attributes for materials that could be used for future design and programming of biohybrid nanomaterial composites with interesting sensor properties.<sup>16</sup> For example, gold nanorings in a size regimen (75–150 nm) similar to those described here were used to detect protein–ligand interactions.<sup>39</sup> Other potential applications include nanorings functioning as storage cavities for proteins or drugs and as near-infrared surface-enhanced spectroscopic sensors.<sup>40,41</sup> Our future studies will explore these applications.

## ■ ASSOCIATED CONTENT

**S Supporting Information.** AuNP synthesis and Figures S1–S3, described in the text. This material is available free of charge via the Internet at <http://pubs.acs.org>.

## ■ AUTHOR INFORMATION

### Corresponding Author

\*E-mail: [smbrozi@sandia.gov](mailto:smbrozi@sandia.gov).

## ■ ACKNOWLEDGMENT

Sandia is a multiprogram laboratory operated by Sandia Corporation, a Lockheed Martin company for the United States Department of Energy under Contract DE-AC04-94AL85000. Work was performed at the Center for Integrated Nanotechnologies, a U.S. Department of Energy, Office of Basic Energy Sciences user facility. We thank Drs. Bruce Bunker and Matt Goertz for helpful discussions.

## ■ REFERENCES

- (1) Sackmann, E. *Science* **1996**, *271*, 43.
- (2) Ranganathan, R. *Science* **2007**, *318*, 1253.
- (3) Cornell, B. A.; Braach-Maksyvtis, V. L. B.; King, L. G.; Osman, P. D. J.; Raguse, B.; Wiczorek, L.; Pace, R. J. *Nature* **1997**, *387*, 580.
- (4) Menger, F. M.; Galloway, A. L.; Chlebowski, M. E.; Wu, S. J. *Am. Chem. Soc.* **2006**, *128*, 14034.
- (5) Hayden, C. C.; Hwang, J. S.; Abate, E. A.; Kent, M. S.; Sasaki, D. Y. *J. Am. Chem. Soc.* **2009**, *131*, 8728.
- (6) Jonsson, M. P.; Jonsson, P.; Dahlin, A. B.; Hook, F. *Nano Lett.* **2007**, *7*, 3462.
- (7) Zwang, T. J.; Fletcher, W. R.; Lane, T. J.; Johal, M. S. *Langmuir* **2010**, *26*, 4598.
- (8) Hartshorn, C. M.; Jewett, C. M.; Brozik, J. A. *Langmuir* **2010**, *26*, 2609.
- (9) Spurlin, T. A.; Gewirth, A. A. *J. Am. Chem. Soc.* **2007**, *129*, 11906.
- (10) Zhang, L. F.; Granick, S. *MRS Bull.* **2006**, *31*, 527.
- (11) Castellana, E. T.; Cremer, P. S. *Surf. Sci. Rep.* **2006**, *61*, 429.
- (12) Roiter, Y.; Ornatska, M.; Rammohan, A. R.; Balakrishnan, J.; Heine, D. R.; Minko, S. *Nano Lett.* **2008**, *8*, 941.
- (13) Tribet, C.; Vial, F. *Soft Matter* **2008**, *4*, 68.
- (14) Denisov, I. G.; McLean, M. A.; Shaw, A. W.; Grinkova, Y. V.; Sligar, S. G. *J. Phys. Chem. B* **2005**, *109*, 15580.
- (15) Li, L.; Lin, M. Y.; Qiu, F.; Yang, Y. L. *Acta Chim. Sin.* **2005**, *63*, 1375.
- (16) Pornpattananankul, D.; Olson, S.; Aryal, S.; Sartor, M.; Huang, C. M.; Vecchio, K.; Zhang, L. *ACS Nano* **2010**, *4*, 1935.
- (17) Roux, M.; Moutard, S.; Perly, B.; Djedaini-Pilard, F. *Biophys. J.* **2007**, *93*, 1620.
- (18) Ginzburg, V. V.; Balijepalli, S. *Nano Lett.* **2007**, *7*, 3716.
- (19) Binder, W. H. *Angew. Chem., Int. Ed.* **2008**, *47*, 3092.
- (20) Wang, B.; Zhang, L. F.; Bae, S. C.; Granick, S. *Proc. Natl. Acad. Sci. U.S.A.* **2008**, *105*, 18171.
- (21) Binder, W. H.; Sachsenhofer, R.; Farnik, D.; Blaas, D. *Phys. Chem. Chem. Phys.* **2007**, *9*, 6435.
- (22) Leroueil, P. R.; Hong, S. Y.; Mecke, A.; Baker, J. R.; Orr, B. G.; Holl, M. M. *Acc. Chem. Res.* **2007**, *40*, 335.
- (23) Windschiegl, B.; Orth, A.; Romer, W.; Berland, L.; Stechmann, B.; Bassereau, P.; Johannes, L.; Steinem, C. *PLoS One* **2009**, *4*, e6238.
- (24) Verma, A.; Stellacci, F. *Small* **2010**, *6*, 12.
- (25) Fang, C.; Fan, Y.; Kong, J. M.; Gao, Z. Q.; Balasubramanian, N. *Appl. Phys. Lett.* **2008**, *92*, 2631081.
- (26) Brust, M.; Walker, M.; Bethell, D.; Schiffrin, D. J.; Whyman, R. *J. Chem. Soc., Chem. Commun.* **1994**, 801.
- (27) Smetana, A. B.; Wang, J. S.; Boeckl, J.; Brown, G. J.; Wai, C. M. *Langmuir* **2007**, *23*, 20429.
- (28) Leroueil, P. R.; Berry, S. A.; Duthie, K.; Han, G.; Rotello, V. M.; McNerny, D. Q.; Baker, J. R.; Orr, B. G.; Holl, M. M. *Nano Lett.* **2008**, *8*, 420.
- (29) Vivares, E.; Ramos, L. *Langmuir* **2005**, *21*, 2185.
- (30) Cambrea, L. R.; Hovis, J. S. *Biophys. J.* **2007**, *92*, 3587.
- (31) Seu, K. J.; Lamberson, E. R.; Hovis, J. S. *J. Phys. Chem. B* **2007**, *111*, 6289.
- (32) Goertz, M. P.; Goyal, N.; Montano, G. A.; Bunker, B. C. *Langmuir* **2011**, *27*, 5481.
- (33) Willets, K. A.; Van Duyne, R. P. *Annu. Rev. Phys. Chem.* **2007**, *58*, 267.
- (34) Haes, A. J.; Van Duyne, R. P. *Anal. Bioanal. Chem.* **2004**, 379, 920.
- (35) Solovkin, A. S.; Tsvetkova, S. V. *Russ. Chem. Rev.* **1962**, *31*, 655.
- (36) Fay, R. C. In *Comprehensive Coordination Chemistry*; Wilkinson, G., Gillard, R. D., McCleverty, J. A., Eds.; Pergamon Press: Oxford, 1987; Chapter 3.
- (37) Willey, G. R.; Woodman, T. J.; Fishes, M. *Transition Met. Chem.* **1998**, *23*, 467.
- (38) Shervedani, R. K.; Bagherzadeh, M. *Biosens. Bioelectron.* **2009**, *24*, 2199.
- (39) Larsson, E. M.; Alegret, J.; Kall, M.; Sutherland, D. S. *Nano Lett.* **2007**, *7*, 1256.
- (40) Sun, Q.; Wang, Q.; Jena, P.; Note, R.; Yu, J. Z.; Kawazoe, Y. *Phys. Rev. B* **2004**, *70*, 245411-1.
- (41) Aizpura, J.; Hanarp, P.; Sutherland, D. S.; Kall, M.; Bryant, G. W.; de Abajo, F. J. G. *Phys. Rev. Lett.* **2003**, *90*, 054701-1.